Dynamical quantum phase transitions in a spin chain with deconfined quantum critical points

Gaoyong Sun [1,*] and Bo-Bo Wei[2,3,†]

[1]*College of Science, Nanjing University of Aeronautics and Astronautics, Nanjing 211106, China*
[2]*School of Science and Engineering, The Chinese University of Hong Kong, Shenzhen, Shenzhen 518172, China*
[3]*Center for Quantum Computing, Peng Cheng Laboratory, Shenzhen 518055, China*

We analytically and numerically study the Loschmidt echo and the dynamical order parameters in a spin chain with a deconfined phase transition between a dimerized state and a ferromagnetic phase. For quenches from a dimerized state to a ferromagnetic phase, we find that the model can exhibit a dynamical quantum phase transition characterized by an associating dimerized order parameter. In particular, when quenching the system from the Majumdar-Ghosh state to the ferromagnetic Ising state, we find an exact mapping into the classical Ising chain for a quench from the paramagnetic phase to the classical Ising phase by analytically calculating the Loschmidt echo and the dynamical order parameters. By contrast, for quenches from a ferromagnetic state to a dimerized state, the system relaxes very fast so that the dynamical quantum transition may exist on only a short timescale. We reveal that the dynamical quantum phase transition can occur in systems with two broken symmetry phases and the quench dynamics may be independent of equilibrium phase transitions.

I. INTRODUCTION

Understanding the behaviors of many-body systems out of equilibrium is a central problem of research in physics [1]. Dynamical quantum phase transitions (DQPTs) [2,3] are proposed to occur at critical times t_c during the real-time evolution with nonanalyticities of the rate function after a sudden quench of the system across equilibrium quantum critical points. Contrary to conversional classical (quantum) phase transitions driven by temperature (magnetic field or pressure), DQPTs are considered new types of phase transitions driven by time. There has been a lot of interest in the study of DQPTs, including critical properties [4–11], dynamical order parameters [12–15], spontaneously broken symmetries [16–21], etc. Realizations of DQPTs have been performed in a large number of experiments based on different platforms [22–29].

On the other hand, the deconfined quantum critical point (DQCP) was originally introduced as a second-order quantum phase transition between the valence bond solid (VBS) state and the antiferromagnetic (AF) Néel phase [30–33]. The lattice symmetry is broken for the VBS phase, while the spin symmetry is broken for the AF phase [30]. A transition between two different broken symmetry phases is usually considered a first-order transition instead of second order according to Landau-Ginzburg-Wilson theory [34,35]. Hence, in two-dimensional models, whether the phase transition is a DQCP or weakly first order is still under debate [33]. Contrary to two-dimensional systems, recent numerical results [36–41] strongly support a continuous second-order transition with the conversional finite-size scaling [39,40] in one-dimensional

models. In this paper, we will focus our study on DQPTs in a one-dimensional spin chain with DQCPs.

Previous studies on DQPTs with spontaneously broken symmetry phases were carried out in many systems (i.e., discrete $\mathbb{Z}_2$ symmetries [16,20], broken continuous symmetries [19], lattice symmetry breaking [21], etc.). Recently, the DQPTs were investigated in a two-dimensional quantum dimer model with VBS phases by considering quenches across a Berezinskii-Kosterlitz-Thouless (BKT) transition and a first-order transition [21]. However, to the best of our knowledge, whether DQPTs can occur in systems after a quench across a DQCP is so far less studied. In the following, we will investigate DQPTs in systems with a quench between two broken symmetry phases based on the Loschmidt echo and dynamical order parameters. We show that DQPTs can occur and be characterized by dimerized order parameters for quenches from VBS phases to ferromagnetic (FM) phases. More importantly, we find that DQPTs in a spin chain with DQCPs for the quench from the Majumdar-Ghosh phase to the classical Ising phase can be mapped to DQPTs in the Ising chain for the quench from the paramagnetic phase to the classical Ising phase.

This paper is organized as follows. In Sec. II, we introduce the concept of the Loschmidt echo. In Sec. III, we discuss the spin chain model with DQCPs we used. In Sec. IV, we review the DQPTs in the transverse field Ising chain. In Sec. V, we present the main results of this paper. In Sec. VI, we summarize.

II. LOSCHMIDT ECHO

Given an initial quantum state $|\psi_0\rangle$, the Loschmidt amplitude $G(t)$ is defined as the overlap between the initial state

---

*Corresponding author: gysun@nuaa.edu.cn
†Corresponding author: weibobo@cuhk.edu.cn

$|\psi_0\rangle$ and its time-evolved states $|\psi(t)\rangle = e^{-iHt}|\psi_0\rangle$,

$$G(t) = \langle\psi_0|e^{-iHt}|\psi_0\rangle, \tag{1}$$

where H is the quench Hamiltonian governing the time evolution of the system. The Loschmidt amplitude can be regarded as a dynamical counterpart of the partition function. Thus, we can define the return rate function,

$$r(t) = -\frac{1}{N}\ln L(t), \tag{2}$$

as an analogy of the free energy of classical systems [2,3]. Here $L(t) = |G(t)|^2$ is the Loschmidt echo, and N is the system size. The rate function will exhibit nonanalytical behaviors (such as a kink structure) at critical times.

III. MODEL

We consider the following spin chain model for the nonequilibrium dynamics proposed recently in [36–40]:

$$H = \sum_j (-J_x \sigma_j^x \sigma_{j+1}^x - J_z \sigma_j^z \sigma_{j+1}^z$$
$$+ K_x \sigma_j^x \sigma_{j+2}^x + K_z \sigma_j^z \sigma_{j+2}^z). \tag{3}$$

Here σ_j^x, σ_j^z are the Pauli matrices at the jth sites; $J_x \geqslant 0$, $J_z \geqslant 0$ and $K_x \geqslant 0$, $K_z \geqslant 0$ are the nearest-neighbor and next-nearest-neighbor coupling constants, respectively. The model has $\mathbb{Z}_2 \times \mathbb{Z}_2$ symmetry, translation symmetry, and inversion symmetry [36]. The system undergoes a second-order quantum phase transition, known as DQCP, between the VBS dimerized phase and the FM phase. We note that (1) for $J_x = J_z = 1$, $K_x = K_z = 1/2$, the ground state is the Majumdar-Ghosh state [37] and (2) for $J_x = K_x = K_z = 0$, $J_z = 1$, the model is reduced to the classical Ising model. In the following, we will study the quench dynamics from the VBS phase to the FM phase and vice versa with periodic boundary conditions (PBCs).

IV. TRANSVERSE FIELD ISING CHAIN

Let us first revisit the DQPTs in the ferromagnetic transverse field Ising chain, which will help us to understand the quench dynamics from the VBS state to the FM phase. The Hamiltonian of the transverse field Ising chain is given by

$$H = -J_z \sum_j \sigma_j^z \sigma_{j+1}^z - h \sum_j \sigma_j^x, \tag{4}$$

with interaction strength $J_z \geqslant 0$ and transverse field $h \geqslant 0$. The system undergoes a second-order quantum phase transition at the critical point $h_c = 1$ between the FM phase for $h < 1$ and the paramagnetic phase for $h > 1$. In particular, the ground state is the classical ferromagnetic phase at $h = 0$ and the fully polarized phase at $h \to \infty$.

We consider the quench from a fully polarized initial state,

$$|\psi_0\rangle = \bigotimes_{j=1}^{N} \frac{1}{\sqrt{2}}(|\uparrow\rangle_j + |\downarrow\rangle_j), \tag{5}$$

which is the eigenstate of the Hamiltonian in Eq. (4) with the transverse field $h \to \infty$, to a final Hamiltonian,

$$H = -J_z \sum_j \sigma_j^z \sigma_{j+1}^z, \tag{6}$$

which corresponds to the Hamiltonian with transverse field $h = 0$ in Eq. (4). Here $|\uparrow\rangle_j$, $|\downarrow\rangle_j$ are the two basis states of σ_j^z denoting spin up and spin down at the jth site. Then the Loschmidt amplitude $G(t)$ in Eq. (1) can be written as

$$G(t) = \langle\psi_0|e^{-iHt}|\psi_0\rangle$$
$$= \langle\psi_0|e^{iJ_z t \sum_j \sigma_j^z \sigma_{j+1}^z}|\psi_0\rangle$$
$$= \frac{1}{2^N}\text{Tr}[e^{iJ_z t \sum_j \sigma_j^z \sigma_{j+1}^z}], \tag{7}$$

where Tr denotes the trace. The Loschmidt amplitude $G(t)$ in Eq. (7) is equivalent to the partition function of the classical Ising model [2,4] by replacing the time t by the inverse temperature β using $it = \beta$; then the Loschmidt amplitude $G(t)$ in Eq. (7) with PBCs becomes

$$G(t) = \text{Tr}[D^N] = \lambda_+^N + \lambda_-^N, \tag{8}$$

where D is the 2×2 matrix

$$D = \frac{1}{2}\begin{pmatrix} e^{iJ_z t} & e^{-iJ_z t} \\ e^{-iJ_z t} & e^{iJ_z t} \end{pmatrix} \tag{9}$$

and $\lambda_+ = \cos(J_z t)$ and $\lambda_- = i\sin(J_z t)$ are the two eigenvalues of matrix D. We can derive the critical times,

$$t_n = \frac{\pi}{4J_z}(2n+1), \tag{10}$$

of the DQPTs by using the condition [2,4]

$$|\lambda_+| = |\lambda_-|, \tag{11}$$

where n are integers. This is equivalent to solving the equation of the Loschmidt amplitude $G(t)$,

$$[\cos(J_z t)]^N + [i\sin(J_z t)]^N = 0, \tag{12}$$

with the condition $N = 4n + 2$ in the domain of real numbers. For $N = 4n$, the critical time t_n in Eq. (10) is obtained by finding the minima of the Loschmidt amplitude $G(t)$, which decreases towards to zero when increasing system size N. Hence, the rate functions in Eq. (2) will diverge for even numbers of system sizes in the limit of $N \to \infty$, indicating DQPTs occur at critical times t_n.

V. SPIN CHAIN WITH DQCP

In this section, we will study the spin chain model with DQCPs defined in Eq. (3) and analytically and numerically present our main results for DQPTs for the quenches from VBS phases to FM phases and vice versa.

For simplicity, In Eq. (3) we choose $J_x = 1$, $K_x = 1/2$, $K_z = 1/2$, and $J_z > 0$ as in Refs. [38–40]. The system exhibits a phase transition from the VBS phase to the FM phase at critical point $J_z^c \approx 1.465$ [38–40]. For $J_z < J_z^c$, the ground state is the VBS phase; for $J_z > J_z^c$, the ground state becomes the FM phase. In particular, at $J_z = 1$, the ground state is the

exact Majumdar-Ghosh state [37],

$$|\psi_0\rangle = \bigotimes_{m=1}^{N/2} \left(\frac{|\uparrow\uparrow\rangle + |\downarrow\downarrow\rangle}{\sqrt{2}} \right)_{2m-1,2m}, \quad (13)$$

where m are integers.

We first consider the quench from the Majumdar-Ghosh state in Eq. (13), which is the eigenstate of the Hamiltonian in Eq. (3) at $J_z = 1$, to the classical Ising phase in Eq. (6) corresponding to the Hamiltonian in Eq. (3) with $J_z \to \infty$. The Loschmidt amplitude $G(t)$ in Eq. (1) now becomes (see Appendix A for details)

$$G(t) = \langle\psi_0|e^{-iHt}|\psi_0\rangle$$

$$= \text{Tr}[D^{N/2}]$$

$$= [\cos(J_z t)]^{N/2} + [i\sin(J_z t)]^{N/2}. \quad (14)$$

This is just the Loschmidt amplitude $G(t)$ of the Ising model as shown in Eq. (8) with system size $N/2$. Hence, DQPTs occur at exactly the same critical times t_n as in Eq. (10) of the transverse field Ising model.

The understanding of this result is as follows. For the case of the transverse field Ising model, the initial state in Eq. (5) is the product state of the eigenstate of single-site operator σ_j^x. In the σ_j^z base, the eigenstate of σ_j^x is the superposition of the spin-up state $|\uparrow\rangle_j$ and the spin-down state $|\downarrow\rangle_j$. Similarly, the Majumdar-Ghosh state is also a product state of the entangled triplet state, as shown in Eq. (13). And the Majumdar-Ghosh state can be regarded as a fully polarized state of system size $N/2$ if each pair in the entangled triplet state is grouped together as a new site, $|\Uparrow\rangle_m = |\uparrow\uparrow\rangle_{2m-1,2m}, |\Downarrow\rangle_m = |\downarrow\downarrow\rangle_{2m-1,2m}$.

In the following, we will show such DQPTs can be described by dimerized order parameters. The dimerized order operators are defined as

$$D_x = \frac{1}{N} \sum_j (-1)^j (\sigma_j^x \sigma_{j+1}^x), \quad (15)$$

$$D_y = \frac{1}{N} \sum_j (-1)^j (\sigma_j^y \sigma_{j+1}^y), \quad (16)$$

$$D_z = \frac{1}{N} \sum_j (-1)^j (\sigma_j^z \sigma_{j+1}^z) \quad (17)$$

in the equilibrium VBS state. Hence, the dynamics of the dimerized order parameters are given by

$$D_x(t) = \langle\Psi(t)|D_x|\Psi(t)\rangle, \quad (18)$$

$$D_y(t) = \langle\Psi(t)|D_y|\Psi(t)\rangle, \quad (19)$$

$$D_z(t) = \langle\Psi(t)|D_z|\Psi(t)\rangle, \quad (20)$$

where $|\Psi(t)\rangle = e^{-iHt}|\Psi_0\rangle$ is the time-evolved state. The dimerized order parameters $D_x(t), D_y(t), D_z(t)$ are evaluated by (see Appendix B for details)

$$D_x(t) = \frac{\cos(2J_z t)^2}{2}, \quad (21)$$

$$D_y(t) = -\frac{\cos(2J_z t)^2}{2}, \quad (22)$$
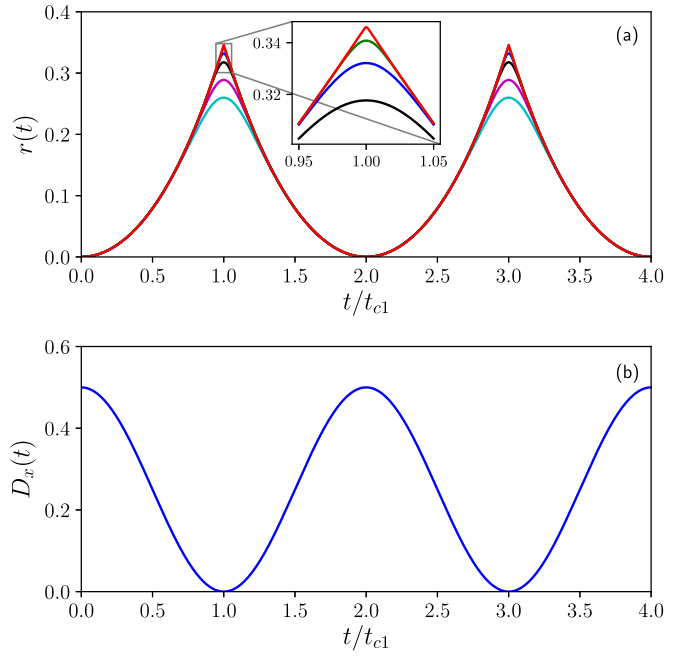
$$D_z(t) = \frac{1}{2}. \quad (23)$$

FIG. 1. Dynamics from the initial Majumdar-Ghosh state to the quenched classical Ising chain of Eq. (3) with time t/t_{c1} and $t_{c1} = \pi/4$. (a) Rate function $r(t)$ for $N = 2400, 240, 96, 48, 24, 16$ lattice sites from top to bottom. The inset in (a) shows the finite-size effects near the first critical time for $L = 2400, 240, 96, 48$ from top to bottom. (b) Dimerized order parameters $D_x(t)$ with the same parameters as (a). The results are the same as the classical Ising model with $N' = N/2$, where the dimerized order parameters $D_x(t)$ corresponds to $\langle\sigma^x(t)\rangle$.

We can see that the dimerized order parameter $D_z(t)$ is conserved during the time evolution, which is due to the fact that the Majumdar-Ghosh state is the eigenstate of the quenched Hamiltonian in Eq. (6), while $D_x(t)$ and $D_y(t)$ vary sinusoidally with time t in the opposite direction. The results of the rate function $r(t)$ and the dimerized order parameters $D_x(t)$ are plotted in Fig. 1, where we can clearly see the kinks in the rate functions, indicating DQPTs occur at $t_n/t_{c1} = (2n + 1)$, as predicted in Eq. (10), with $t_{c1} = \frac{\pi}{4}$ being the first critical time. We find that DQPTs can be described by x-component dimerized order parameters $D_x(t)$ [or y-component $D_y(t)$], which become zero at critical time t_n [42]. Interestingly, the value of the x-component dimerized order parameters $D_x(t)$ is just half of the value of $\langle\sigma^x(t)\rangle$ in the transverse field Ising chain. It supported our argument again that we can group the two entangled particles together and consider their dynamics to be that in the Ising model.

Indeed, the above arguments and results for the Loschmidt amplitude $G(t)$ can be generated to any product state consisting of a K-qubit Greenberger-Horne-Zeilinger (GHZ) state,

$$|\psi_0\rangle = \bigotimes_{m=1}^{N/K} \left(\frac{|\uparrow\rangle^{\otimes K} + |\downarrow\rangle^{\otimes K}}{\sqrt{2}} \right)_{Km-K+1,...,Km}. \quad (24)$$

The Loschmidt amplitude $G(t)$ for the initial K-qubit GHZ state would become

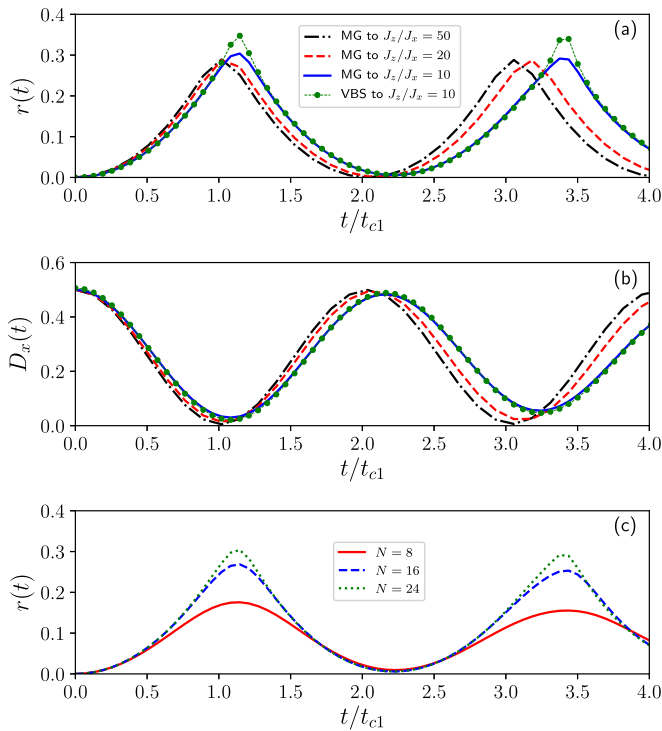$$G(t) = [\cos(J_z t)]^{N/K} + [i\sin(J_z t)]^{N/K} \quad (25)$$

FIG. 2. Dynamics from the initial VBS phases to FM phases of Eq. (3) with time t/t_{c1} and $t_{c1} = \pi/4$. (a) Rate function $r(t)$ of $N = 24$ lattice sites for the quench from the Majumdar-Ghosh (MG) phase at $J_z/J_x = 1$ to the FM phase at $J_z/J_x = 50$ (black dash-dotted line), $J_z/J_x = 20$ (red dashed line), $J_z/J_x = 10$ (blue solid line). The green solid circles denote the data for the quench from the VBS phase at $J_z/J_x = 1.05$ to the FM phase at $J_z/J_x = 10$ with $N = 24$ lattice sites. The results change little compared to that for the quench from the MG state to the FM phase at $J_z/J_x = 10$. (b) Dimerized order parameters $D_x(t)$ with the same parameters as (a). (c) The finite-size scaling of the rate function $r(t)$ for the quench from the MG phase to the FM phase at $J_z/J_x = 10$ with $N = 8$ (red solid line), $N = 16$ (blue dashed line), $N = 24$ (green dotted line) lattice sites. We rescale the Hamiltonian by choosing $J_z = 1$ in the simulations.

if we grouped the K-qubit GHZ state as a new single-lattice size. We numerically confirm the above analytical results of the Loschmidt amplitude $G(t)$ by using the exact diagonalization for GHZ states in small systems.

Next, let us start to consider the general quenches from the Majumdar-Ghosh state $J_z = 1$ to FM states (large but finite J_z) by increasing J_z from $J_z \to \infty$. For very large J_z, where the fluctuations are weak, we expect that the DQPTs will survive. To support our argument, we perform the exact diagonalization up to $N = 24$ lattice size for $J_z/J_x = 50$, $J_z/J_x = 20$, and $J_z/J_x = 10$ in PBCs. The rate function $r(t)$ and x-component dimerized order parameters $D_x(t)$ are presented in Fig. 2. For very large $J_z = 50$, the rate function $r(t)$ and order parameters $D_x(t)$ change little compared to the classical Ising model. Increasing J_z, the peak of rate functions $r(t)$ and minima of order parameters $D_x(t)$ move in the right direction due to the stronger fluctuations in the quenched Hamiltonian. We find the peaks of the rate functions $r(t)$ increase with system size around the local minima of the order parameters $D_x(t)$, indicating that DQPTs persist even for $J_z/J_x = 10$ [see Fig. 2(c)].
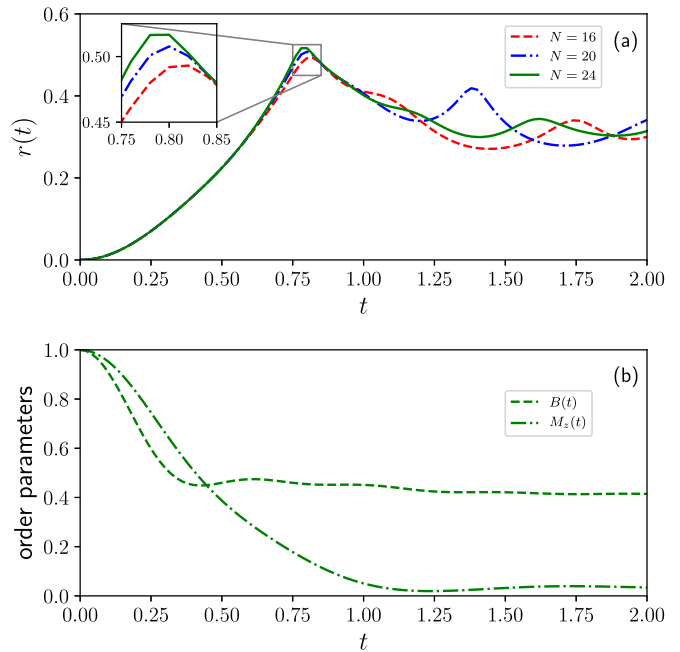

FIG. 3. Dynamics from the initial fully polarized FM phases ($N \to \infty$) to the Majumdar-Ghosh phase $J_z = 1$ of Eq. (3) with time t. (a) Rate function $r(t)$ for $N = 16$ (red dashed line), $N = 20$ (blue dash-dotted line), $N = 24$ (green solid line) lattice sites. The inset in (a) denotes the finite-size effects near the first critical time. (b) Bond order parameters $B(t)$ (dashed line) and the magnetization $M_z(t)$ (dash-dotted line) with $N = 24$ sites.

And the existence of DQPTs is robust under a small perturbation of the initial Majumdar-Ghosh state [i.e., changing $J_z/J_x = 1$ to $J_z/J_x = 1.05$; see Fig. 2(a)]. We note that when J_z is close to the equilibrium critical point $J_z^c \approx 1.465$, we cannot find nice kinks due to the strong fluctuations where the criticality of the DQCP plays an important role in the DQPTs. The study of the quenches near the critical point is a very difficult problem that we leave for future work.

Finally, we will briefly discuss the DQPTs from the quenches from the fully polarized FM phase ($J_z \to \infty$) to the Majumdar-Ghosh state ($J_z = 1$). We quench our system from one of the doubly degenerate polarized FM phases

$$|\psi_0\rangle = \bigotimes_{i=1}^{N}(|\uparrow\rangle_i) \qquad (26)$$

to the Majumdar-Ghosh model and perform the exact diagonalization to compute the rate functions $r(t)$, bond order parameters $B(t) = \langle \vec{\sigma}_i \cdot \vec{\sigma}_{i+1} \rangle$, and magnetization $M_z(t) = \frac{1}{N} \sum_i \langle \sigma_i^z \rangle$ in PBCs. The results are shown in Fig. 3, where we can see that the bond order parameters $B(t)$ and the magnetization $M_z(t)$ decay very quickly to equilibrium values of $B(t) \approx 1/2$ and $M_z(t) \approx 0$ so that it is very difficult to denote the DQPTs, although it seem that there is a DQPT (kink structure) on the short timescale. We note that our result in this case is different from that in the XXZ model [16], where the magnetization shows an oscillatory behavior and DQPTs can be well described by comparing two rate functions $r_\eta(t)$, with η denoting two degenerate Néel phases. Therefore, our results reveal that different broken symmetries will play a different

role in the quench dynamics. It would be very interesting to understand the relations between DQPTs and symmetries in the future.

VI. CONCLUSION

In this paper, we studied the quench dynamics in a spin chain with a DQCP. We derived analytical results of the Loschmidt amplitude and order parameters for the quench from the Majumdar-Ghosh state to the classical Ising chain. For more general cases, we numerically investigated the quench dynamics. We showed that DQPTs can occur in systems with two broken symmetry phases and can be described by x-component (or y-component) dimerized VBS order parameters. Our results reveal that broken lattice symmetry and broken spin symmetry of the quenched Hamiltonian play a different role in the quench dynamics. For the quench from the broken lattice symmetry to the $\mathbb{Z}_2$ broken classical Ising chain, we found that the dynamics of Loschmidt amplitude with the initial Majumdar-Ghosh state is equivalent to a product state of a translation symmetry. This means we cannot distinguish the Ising transition and the DQCP from such quench dynamics, implying that one should consider the quenches near the DQCP in order to study its critical properties [43–45]. We note that our results for the initial VBS states and any K-qubit GHZ states have been realized in recent experiments [46].

It would be very interesting to investigate the quench dynamics in two-dimensional systems with DQCPs to know whether DQPTs can occur and whether the dynamics of the Loschmidt amplitude can be mapped to the two-dimensional classical Ising model.

ACKNOWLEDGMENTS

APPENDIX A: DERIVATION OF LOSCHMIDT AMPLITUDE

To investigate the DQPTs in the system, we start with the dimerized Majumdar-Ghosh state, which is given by

$$|\Psi_0\rangle = \bigotimes_{m=1}^{N/2} \left(\frac{|\uparrow\uparrow\rangle + |\downarrow\downarrow\rangle}{\sqrt{2}} \right)_{2m-1,2m}, \quad (A1)$$

where $|\uparrow, \downarrow\rangle$ are the basis state along the z direction. We then quench this state by a Hamiltonian deep in the z-FM regime with $J_z \gg 1$, which is

$$H = -\sum_{i=1}^{N} J_z \sigma_i^z \sigma_{i+1}^z. \quad (A2)$$

To evaluate the Loschmidt echo, we note that

$$\begin{aligned}|\Psi(t)\rangle &= e^{-itH}|\Psi_0\rangle \\ &= \prod_i e^{itJ_z \sigma_i^z \sigma_{i+1}^z}|\Psi_0\rangle \\ &= e^{itJ_z N/2} \prod_{i=2,4,\cdots,2m} e^{itJ_z \sigma_i^z \sigma_{i+1}^z}|\Psi_0\rangle. \quad (A3)\end{aligned}$$

If we group each pair in the entangled triplet state as a new site,

$$|\Uparrow\rangle_m = |\uparrow\uparrow\rangle_{2m-1,2m}, \quad |\Downarrow\rangle_m = |\downarrow\downarrow\rangle_{2m-1,2m}, \quad (A4)$$

the Majumdar-Ghosh state in Eq. (A1) becomes

$$|\psi_0\rangle = \bigotimes_{m=1}^{N/2} \frac{1}{\sqrt{2}}(|\Uparrow\rangle_m + |\Downarrow\rangle_m). \quad (A5)$$

The eigenvalue equations of operators

$$\sigma_{2m}^z = \mathbb{1}_{2m-1} \otimes \sigma_{2m}^z, \quad (A6)$$

$$\sigma_{2m+1}^z = \sigma_{2m+1}^z \otimes \mathbb{1}_{2m+2} \quad (A7)$$

are

$$\sigma_{2m}^z|\psi_0\rangle = \frac{1}{\sqrt{2}}(|\Uparrow\rangle_m - |\Downarrow\rangle_m), \quad (A8)$$

$$\sigma_{2m+1}^z|\psi_0\rangle = \frac{1}{\sqrt{2}}(|\Uparrow\rangle_m - |\Downarrow\rangle_m), \quad (A9)$$

which are the same as the Ising model. Then the Loschmidt amplitude for PBCs is

$$\begin{aligned}G(t) &= \langle\Psi_0|e^{-itH}|\Psi_0\rangle \\ &= \langle\Psi_0|e^{itJ_z N/2} \prod_{i=2,4,...,2m} e^{itJ_z \sigma_i^z \sigma_{i+1}^z}|\Psi_0\rangle \\ &= \text{Tr}[D^{N/2}] \\ &= [\cos(J_z t)]^{N/2} + [i\sin(J_z t)]^{N/2}. \quad (A10)\end{aligned}$$

APPENDIX B: DERIVATION OF ORDER PARAMETERS

Now let us first see how the polarizations $\langle\sigma^x\rangle$ in the x direction evolve in the classical Ising model for PBCs,

$$\begin{aligned}\langle\sigma^x(t)\rangle &= \frac{1}{N}\left\langle \sum_j \sigma_j^x \right\rangle = \frac{1}{N}\langle\Psi_0|e^{-iJ_z t \sum_i \sigma_i^z \sigma_{i+1}^z} \sum_j \sigma_j^x e^{iJ_z t \sum_i \sigma_i^z \sigma_{i+1}^z}|\Psi_0\rangle = \langle\Psi_0|e^{-iJ_z t \sum_i \sigma_i^z \sigma_{i+1}^z} \sigma_1^x e^{iJ_z t \sum_i \sigma_i^z \sigma_{i+1}^z}|\Psi_0\rangle \\ &= \langle\Psi_0|e^{-iJ_z t \sum_{i=2}^{N-1} \sigma_i^z \sigma_{i+1}^z} e^{-iJ_z t \sigma_1^z(\sigma_N^z + \sigma_2^z)} \sigma_1^x e^{iJ_z t \sigma_1^z(\sigma_N^z + \sigma_2^z)} e^{iJ_z t \sum_{i=2}^{N-1} \sigma_i^z \sigma_{i+1}^z}|\Psi_0\rangle = \langle\Psi_0|e^{-iJ_z t \sum_{i=2}^{N-1} \sigma_i^z \sigma_{i+1}^z} \{\sigma_1^x \cos[2J_z t(\sigma_N^z + \sigma_2^z)] \\ &\quad + \sigma_1^y \sin[2J_z t(\sigma_N^z + \sigma_2^z)]\} e^{iJ_z t \sum_{i=2}^{N-1} \sigma_i^z \sigma_{i+1}^z}|\Psi_0\rangle = \langle\Psi_0|e^{-iJ_z t \sum_{i=2}^{N-1} \sigma_i^z \sigma_{i+1}^z} \{\cos[2J_z t(\sigma_N^z + \sigma_2^z)]\} e^{iJ_z t \sum_{i=2}^{N-1} \sigma_i^z \sigma_{i+1}^z}|\Psi_0\rangle \\ &= \cos^2(2J_z t). \end{aligned} \quad (B1)$$

Next, we will show the details of computing the dimerized order parameters $\langle D_x(t)\rangle$, $\langle D_y(t)\rangle$, $\langle D_z(t)\rangle$ defined in Eqs. (18), (19), and (20). The order parameter dynamics $\langle D_z(t)\rangle$ can be easily calculated as

$$\langle D_z(t)\rangle = \langle\Psi_0|e^{itH}D_z e^{-itH}|\Psi_0\rangle = \langle\Psi_0|D_z|\Psi_0\rangle = \frac{1}{2}. \tag{B2}$$

To evaluate $\langle D_x(t)\rangle$ and $\langle D_y(t)\rangle$, we note that the quenched state has the form

$$|\Psi(t)\rangle = e^{itJ_z N/2} e^{iJ_z t \sum\limits_{i=2,4,\ldots,2m} \sigma_i^z \sigma_{i+1}^z}|\Psi_0\rangle. \tag{B3}$$

Thus, we have

$\langle\Psi(t)|\sigma_1^x\sigma_2^x|\Psi(t)\rangle$

$= \langle\Psi_0|e^{-iJ_z t \sum\limits_{i=\mathrm{even}} \sigma_i^z\sigma_{i+1}^z} \sigma_1^x\sigma_2^x e^{iJ_z t \sum\limits_{i=\mathrm{even}} \sigma_i^z\sigma_{i+1}^z}|\Psi_0\rangle = \langle\Psi_0|e^{-iJ_z t\sum_{i=4}^{2m-2}\sigma_i^z\sigma_{i+1}^z} e^{-iJ_z t(\sigma_2^z\sigma_3^z + \sigma_1^z\sigma_N^z)}\sigma_1^x\sigma_2^x e^{iJ_z t(\sigma_1^z\sigma_N^z + \sigma_2^z\sigma_3^z)} e^{iJ_z t\sum_{i=4}^{2m-2}\sigma_i^z\sigma_{i+1}^z}|\Psi_0\rangle$

$= \langle\Psi_0|e^{-iJ_z t\sum_{i=4}^{2m-2}\sigma_i^z\sigma_i^{z+1}}\{\sigma_1^x\sigma_2^x \cos[2J_z t(\sigma_N^z)]\cos[2J_z t(\sigma_3^z)] + \sigma_1^y\sigma_2^y \sin[2J_z t(\sigma_N^z)]\sin[2J_z t(\sigma_3^z)]\}e^{iJ_z t\sum_{i=4}^{2m-2}\sigma_i^z\sigma_i^{z+1}}|\Psi_0\rangle = \cos^2(2J_z t). \tag{B4}$

Similarly, we have

$$\langle\Psi(t)|\sigma_2^x\sigma_3^x|\Psi(t)\rangle = 0, \tag{B5}$$

$$\langle\Psi(t)|\sigma_3^x\sigma_4^x|\Psi(t)\rangle = \cos^2(2J_z t), \tag{B6}$$

$$\langle\Psi(t)|\sigma_4^x\sigma_5^x|\Psi(t)\rangle = 0. \tag{B7}$$

Finally, we get

$$\langle D_x(t)\rangle = \langle\Psi(t)|D_x|\Psi(t)\rangle = \frac{\cos^2(2J_z t)}{2}, \tag{B8}$$

$$\langle D_y(t)\rangle = \langle\Psi(t)|D_y|\Psi(t)\rangle = -\frac{\cos^2(2J_z t)}{2}. \tag{B9}$$

[1] J. Eisert, M. Friesdorf, and C. Gogolin, Nat. Phys. **11**, 124 (2015).

[2] M. Heyl, A. Polkovnikov, and S. Kehrein, Phys. Rev. Lett. **110**, 135704 (2013).

[3] M. Heyl, Rep. Prog. Phys. **81**, 054001 (2018).

[4] M. Heyl, Phys. Rev. Lett. **115**, 140602 (2015).

[5] C. Karrasch and D. Schuricht, Phys. Rev. B **95**, 075143 (2017).

[6] D. V. Chichinadze and A. N. Rubtsov, Phys. Rev. B **95**, 180302(R) (2017).

[7] A. Khatun and S. M. Bhattacharjee, Phys. Rev. Lett. **123**, 160603 (2019).

[8] Y. Wu, Phys. Rev. B **101**, 014305 (2020).

[9] Y. Wu, Phys. Rev. B **101**, 064427 (2020).

[10] Y. Wu, arXiv:1908.04476.

[11] D. Trapin, J. C. Halimeh, and M. Heyl, arXiv:2005.06481.

[12] J. C. Budich and M. Heyl, Phys. Rev. B **93**, 085416 (2016).

[13] S. Sharma, U. Divakaran, A. Polkovnikov, and A. Dutta, Phys. Rev. B **93**, 144306 (2016).

[14] U. Bhattacharya and A. Dutta, Phys. Rev. B **96**, 014302 (2017).

[15] M. Heyl and J. C. Budich, Phys. Rev. B **96**, 180304(R) (2017).

[16] M. Heyl, Phys. Rev. Lett. **113**, 205701 (2014).

[17] E. Canovi, P. Werner, and M. Eckstein, Phys. Rev. Lett. **113**, 265702 (2014).

[18] T. Fogarty, A. Usui, T. Busch, A. Silva, and J. Goold, New J. Phys. **19**, 113018 (2017).

[19] S. A. Weidinger, M. Heyl, A. Silva, and M. Knap, Phys. Rev. B **96**, 134313 (2017).

[20] Y.-P. Huang, D. Banerjee, and M. Heyl, Phys. Rev. Lett. **122**, 250401 (2019).

[21] J. Feldmeier, F. Pollmann, and M. Knap, Phys. Rev. Lett. **123**, 040601 (2019).

[22] P. Jurcevic, H. Shen, P. Hauke, C. Maier, T. Brydges, C. Hempel, B. P. Lanyon, M. Heyl, R. Blatt, and C. F. Roos, Phys. Rev. Lett. **119**, 080501 (2017).

[23] N. Fläschner, D. Vogel, M. Tarnowski, B. Rem, D.-S. Lühmann, M. Heyl, J. Budich, L. Mathey, K. Sengstock, and C. Weitenberg, Nat. Phys. **14**, 265 (2018).

[24] X.-Y. Xu, Q.-Q. Wang, M. Heyl, J. C. Budich, W.-W. Pan, Z. Chen, M. Jan, K. Sun, J.-S. Xu, Y.-J. Han, C.-F. Li, and G.-C. Guo, Light: Sci. Appl. **9**, 1 (2020).

[25] K. Wang, X. Qiu, L. Xiao, X. Zhan, Z. Bian, W. Yi, and P. Xue, Phys. Rev. Lett. **122**, 020501 (2019).

[26] T. Tian, Y. Ke, L. Zhang, S. Lin, Z. Shi, P. Huang, C. Lee, and J. Du, Phys. Rev. B **100**, 024310 (2019).

[27] X.-Y. Guo, C. Yang, Y. Zeng, Y. Peng, H.-K. Li, H. Deng, Y.-R. Jin, S. Chen, D. Zheng, and H. Fan, Phys. Rev. Appl. **11**, 044080 (2019).

[28] X. Nie, B.-B. Wei, X. Chen, Z. Zhang, X. Zhao, C. Qiu, Y. Tian, Y. Ji, T. Xin, D. Lu, and J. Li, Phys. Rev. Lett. **124**, 250601 (2020).

[29] T. Tian, H.-X. Yang, L.-Y. Qiu, H.-Y. Liang, Y.-B. Yang, Y. Xu, and L.-M. Duan, Phys. Rev. Lett. **124**, 043001 (2020).

[30] T. Senthil, A. Vishwanath, L. Balents, S. Sachdev, and M. P. A. Fisher, Science **303**, 1490 (2004).

[31] T. Senthil, L. Balents, S. Sachdev, A. Vishwanath, and M. P. A. Fisher, Phys. Rev. B **70**, 144407 (2004).

[32] A. W. Sandvik, Phys. Rev. Lett. **98**, 227202 (2007).

[33] H. Shao, W. Guo, and A. W. Sandvik, Science **352**, 213 (2016).

[34] K. G. Wilson and J. Kogut, Phys. Rep. **12**, 75 (1974).

[35] K. G. Wilson, Rev. Mod. Phys. **47**, 773 (1975).

[36] S. Jiang and O. Motrunich, Phys. Rev. B **99**, 075103 (2019).

[37] B. Roberts, S. Jiang, and O. I. Motrunich, Phys. Rev. B **99**, 165143 (2019).

[38] R.-Z. Huang, D.-C. Lu, Y.-Z. You, Z. Y. Meng, and T. Xiang, Phys. Rev. B **100**, 125137 (2019).

[39] Q. Luo, J. Zhao, and X. Wang, Phys. Rev. B **100**, 121111(R) (2019).

[40] G. Sun, B.-B. Wei, and S.-P. Kou, Phys. Rev. B **100**, 064427 (2019).

[41] C. Mudry, A. Furusaki, T. Morimoto, and T. Hikihara, Phys. Rev. B **99**, 205153 (2019).

[42] I. Hagymási, C. Hubig, Ö. Legeza, and U. Schollwöck, Phys. Rev. Lett. **122**, 250601 (2019).

[43] B. Zhou, C. Yang, and S. Chen, Phys. Rev. B **100**, 184313 (2019).

[44] M.-J. Hwang, B.-B. Wei, S. F. Huelga, and M. B. Plenio, arXiv:1904.09937.

[45] C. Ding, Phys. Rev. B **102**, 060409(R) (2020).

[46] C. Song, K. Xu, H. Li, Y.-R. Zhang, X. Zhang, W. Liu, Q. Guo, Z. Wang, W. Ren, J. Hao, H. Feng, H. Fan, D. Zheng, D.-W. Wang, H. Wang, and S. Zhu, Science **365**, 574 (2019).